Predictability of El Niño Duration Based on the Onset Timing

XIAN WU,[a] YUKO M. OKUMURA,[a] AND PEDRO N. DINEZIO[a]

[a] *Institute for Geophysics, Jackson School of Geosciences, The University of Texas at Austin, Austin, Texas*

(Manuscript received 19 December 2019, in final form 25 September 2020)

ABSTRACT: Analysis of observational data and a long control simulation of the Community Earth System Model, version 1 (CESM1), shows that El Niño events developing in boreal spring to early summer usually terminate after peaking in winter, whereas those developing after summer tend to persist into the second year. To test the predictability of El Niño duration based on the onset timing, perfect model predictions were conducted for three El Niño events developing in April or September in the CESM1 control simulation. For each event, 30-member ensemble simulations are initialized with the same oceanic conditions in the onset month but with slightly different atmospheric conditions and integrated for 2 years. The CESM1 successfully predicts the termination of El Niño after the peak in 95% of the April-initialized simulations and the continuation of El Niño into the second year in 83% of the September-initialized simulations. The predictable component of El Niño duration arises from the initial oceanic conditions that affect the timing and magnitude of negative feedback within the equatorial Pacific, as well as from the Indian and Atlantic Oceans. The ensemble spread of El Niño duration, on the other hand, originates from surface wind variability over the western equatorial Pacific in spring following the peak. The wind variability causes a larger spread in the September-initialized than the April-initialized ensemble simulations due to weaker negative feedback in spring. These results indicate potential predictability of El Niño events beyond the current operational forecasts by 1 year.

KEYWORDS: Pacific Ocean; Atmosphere-ocean interaction; El Nino; ENSO; Climate prediction; Climate models

1. Introduction

The El Niño–Southern Oscillation (ENSO) phenomenon is the dominant mode of interannual climate variability arising from dynamic and thermodynamic interactions of the tropical ocean and atmosphere (e.g., Wallace et al. 1998; Neelin et al. 1998; Wang and Picaut 2004; Chang et al. 2006; Capotondi et al. 2015; Timmermann et al. 2018; Okumura 2019; McPhaden et al. 2020). The warm (El Niño) and cold (La Niña) phases of ENSO typically last 1–2 years and influence global weather patterns via atmospheric teleconnections (e.g., Trenberth et al. 1998; Alexander et al. 2002). Predicting the state of ENSO is thus critical for global climate predictions on seasonal to interannual time scales (e.g., Kumar and Hoerling 2000; Shukla et al. 2000; Kumar et al. 2014; Scaife et al. 2014; L'Heureux et al. 2015, 2020). Previous studies of ENSO predictions focus on predicting the onset and amplitude of El Niño events (Latif et al. 1998; Kirtman et al. 2002; Chen and Cane 2008; Jin et al. 2008). Predicting the *duration* of El Niño and La Niña events has received less research attention, despite the severe climate impact of ENSO events lasting 2 or more years. For example, multiyear La Niña events cause persistent drought conditions over the southern tier of the United States (Hoerling and Kumar 2002; Seager and Hoerling 2014; Rippey 2015; Okumura et al. 2017). It is therefore important to predict the occurrence of multiyear ENSO events with sufficient lead times. However, the current operational ENSO forecasts are limited to lead times up to 12 months (Barnston et al. 2012, 2019), precluding the predictions of multiyear ENSO events.

Analysis of observational data shows that about one-third of El Niño events and half of La Niña events lasted 2 years or longer since 1900 (Wu et al. 2019). The higher fraction of multiyear events for La Niña than El Niño is consistent with the overall asymmetry in their duration (Kessler 2002; Larkin and Harrison 2002; McPhaden and Zhang 2009; Ohba and Ueda 2009; Okumura and Deser 2010; Wu et al. 2010). Recent studies suggest that the duration of La Niña events is strongly affected by the amplitude of preceding El Niño (DiNezio et al. 2017a; Wu et al. 2019). La Niña events preceded by strong El Niño tend to last multiple years due to large initial discharge of the equatorial oceanic heat content, as well as delayed adjustments of the tropical Indian and Atlantic Oceans to La Niña (DiNezio and Deser 2014; DiNezio et al. 2017a; Wu et al. 2019). This mechanism explains the high predictability of multiyear La Niña events, particularly those following a strong El Niño (DiNezio et al. 2017a,b). Other factors, such as the state of the tropical Indian and Atlantic Oceans, could also affect the predictions of multiyear La Niña event in 2010–12 (Luo et al. 2017).

The duration of El Niño events, on the other hand, appears to be linked to the timing of their onset (Horii and Hanawa 2004; Lee et al. 2014; Wu et al. 2019). In a composite analysis based on observations and a long control simulation of the Community Earth System Model, version 1 (CESM1), El Niño events developing in boreal spring to early summer usually terminate after peaking in winter, whereas El Niño events

Denotes content that is immediately available upon publication as open access.

Supplemental information related to this paper is available at the Journals Online website: https://doi.org/10.1175/JCLI-D-19-0963.s1.

Corresponding author: Dr. Xian Wu, xianwu@ucar.edu

DOI: 10.1175/JCLI-D-19-0963.1

developing after summer tend to be weaker and persist into the second year (Figs. 1a,c; see section 2 for the definition of El Niño events; Wu et al. 2019). Despite the overall linear relationship between the El Niño duration and the onset month, individual El Niño events exhibit diverse duration, particularly for late-onset months (Figs. 1b,d). Wu et al. (2019) suggest that the onset timing of an El Niño event controls the timing and strength of the delayed negative feedback responsible for its termination not only within the equatorial Pacific but also from the tropical Indian and Atlantic Oceans via atmospheric teleconnections. They also attribute the diverse duration of individual events to remote influences from the tropical Indian and Atlantic Oceans, as well as from the North Pacific. In addition to the timing of oceanic and atmospheric adjustments, the large amplitude of early-onset El Niño events may also lead to nonlinear atmospheric response that hastens the event termination (Harrison and Vecchi 1999; Lengaigne et al. 2006; Okumura et al. 2011; Wu et al. 2010; McGregor et al. 2013).

It remains unknown whether the duration of El Niño events is predictable. Here we address this question by performing idealized prediction experiments with the CESM1, a model that simulates a realistic relationship between El Niño duration and onset timing. We select El Niño events that develop early (April) and late (September) from the control simulation of CESM1 and generate ensemble predictions of these events. The oceanic and atmospheric processes responsible for the predictable (i.e., ensemble mean) and unpredictable (i.e., ensemble spread) components of the ensemble predictions are analyzed in detail. In addition to the onset timing, the impact of El Niño amplitude on the event duration is examined using ensembles initialized with different magnitude of oceanic anomalies.

The rest of the paper is organized as follows. Section 2 describes the model used in this study and the methodology of perfect model experiments. The predictability of El Niño duration and underlying mechanisms are analyzed using the perfect model experiments in section 3. Section 4 summarizes the main results and discusses the implications for future studies.

2. Model and experiments

a. ENSO simulation in CESM1

The CESM1 is a state-of-the-art climate model developed at the National Center for Atmospheric Research and comprising atmosphere, ocean, land surface, and sea ice components (Hurrell et al. 2013; Kay et al. 2015). The atmospheric component, the Community Atmosphere Model, version 5 (CAM5), uses a finite-volume dynamical core on a latitude–longitude grid at horizontal resolutions of 0.9° latitude × 1.25° longitude with 26 levels in vertical. The CAM5 has updated schemes of physical parameterization, including moist turbulence, cloud macrophysics, longwave and shortwave radiative transfer, and aerosol formations compared to its predecessor (Neale et al. 2012). The oceanic component is the Parallel Ocean Program, version 2 (Smith et al. 2010) that has meridional resolution increasing from 0.65° at 60°N to 0.27° at the equator and 60 levels in the vertical.

The CESM1 reproduces many key features of tropical Pacific mean climate and variability. The simulated ENSO shows a broad spectral peak in a 3–6-yr band and diverse amplitude and pattern of events as in observations, although the amplitude of ENSO is overestimated by 18% in CESM1 (0.91°C) compared to observations (0.77°C) based on the standard deviation of monthly SST anomaly averaged in the Niño-3.4 region (5°S–5°N, 170°–120°W; hereafter the Niño-3.4 index). The CESM1 also reproduces the observed asymmetries in the amplitude, pattern, and duration of El Niño and La Niña (DiNezio et al. 2017a). Importantly, the relative frequency of single- and multiyear events and the associated oceanic and atmospheric processes are realistically simulated for both El Niño and La Niña in CESM1 (Wu et al. 2019). Multiyear El Niño events in CESM1 tend to begin with weak equatorial warming in the first year and develop into strong El Niño in the second year (DiNezio et al. 2017a; Wu et al. 2019). In observation, the two peaks of multiyear El Niño events show comparable amplitude, except for a recent multiyear El Niño in 2014–16. This model has been used to successfully predict the duration of La Niña events (DiNezio et al. 2017a,b).

b. Perfect model experiments

The perfect model experiments are based on three El Niño events taken from a 2200-yr preindustrial control simulation of CESM1 conducted as part of the CESM Large Ensemble Project (Kay et al. 2015). We use model years 400–2200, for which the model exhibits negligible global SST trend. El Niño events are defined when the Niño-3.4 index is greater than 0.75 standard deviations in any months between October and February but less than 0.5°C in December of the previous year. The standard deviation of the Niño-3.4 index is calculated separately for each month, ranging from 1.00° to 1.17°C during October–February. The criterion used for the previous year is slightly different from Wu et al. (2019), but this difference does not affect the fundamental results shown in Fig. 1. The year when the El Niño event first develops is denoted as year 0 and the months of that year as Jan^0, Feb^0, . . . , Dec^0. We use the Dec^{+1} Niño-3.4 index as a proxy for the El Niño duration. When the Dec^{+1} Niño-3.4 index is above 0.5°C, El Niño is defined as a multiyear event, otherwise as a single year event. The onset month is defined as the month when the Niño-3.4 index first exceeds 0.5°C. We note that in the CESM1 control simulation there is a very high chance of El Niño development (>80%) once the Niño-3.4 index exceeds 0.5°C (not shown). As we will show later, simulations initialized with this condition almost always develop into El Niño in the first year.

To investigate the predictability of El Niño duration based on the onset timing, we perform ensemble predictions of two early-onset El Niño events that developed in April of model years 1729 and 1686, and one late-onset El Niño event that developed in September of model year 1236. Note that 82% of El Niño events develop between April and September in the CESM1 control simulation, with the most frequent onset in July (28%; see the statistics shown under the bottom color bar in Fig. 1). These selected April- and September-onset El Niño events terminated and persisted in year 1 in the control simulation, respectively, consistently with the composite analysis

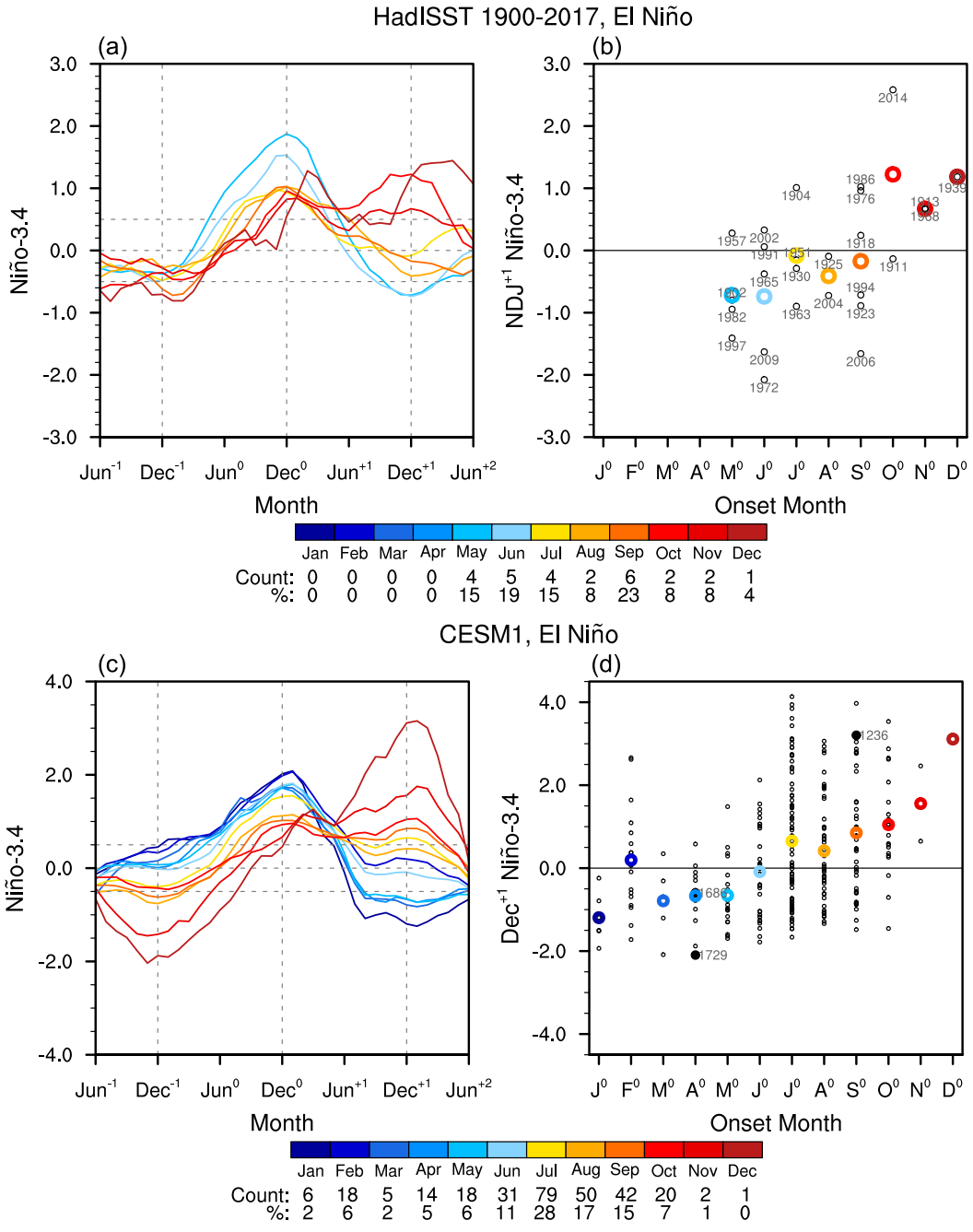

FIG. 1. (a) Time series of the Niño-3.4 index (°C) from Jun^{-1} to Jun^{+2} composited for El Niño events categorized by the onset month and (b) scatterplots of the onset month vs the Dec^{+1} Niño-3.4 index for El Niño events based on the Hadley Centre Sea Ice and SST (HadISST) dataset for 1900–2017 (Rayner et al. 2003). (c),(d) As in (a) and (b), but for the CESM1 control simulation for model years 400–2200. In (a) and (c), the color of composite curves corresponds to the onset month as shown in color bars. The numbers under the color bars indicate the count and percentage of events used in individual composites. In (b) and (d), small black circles indicate individual events and large colored circles represent composites based on the onset month. The three El Niño events in the CESM1 control simulation used for the perfect model experiments are labeled by model years. The HadISST Niño-3.4 index is smoothed with a 3-month running-mean filter.

stratified by onset month (Fig. 1d). For each case, we conducted 30-member ensemble simulations initialized with the same oceanic, sea ice, and land conditions on the first day of the onset month but with slightly different atmospheric conditions. All simulations were integrated for 2 years to explore the long-term predictability. The atmospheric initial conditions were generated by perturbing the temperature, wind, and moisture fields on the first day of the onset month with a round-off level

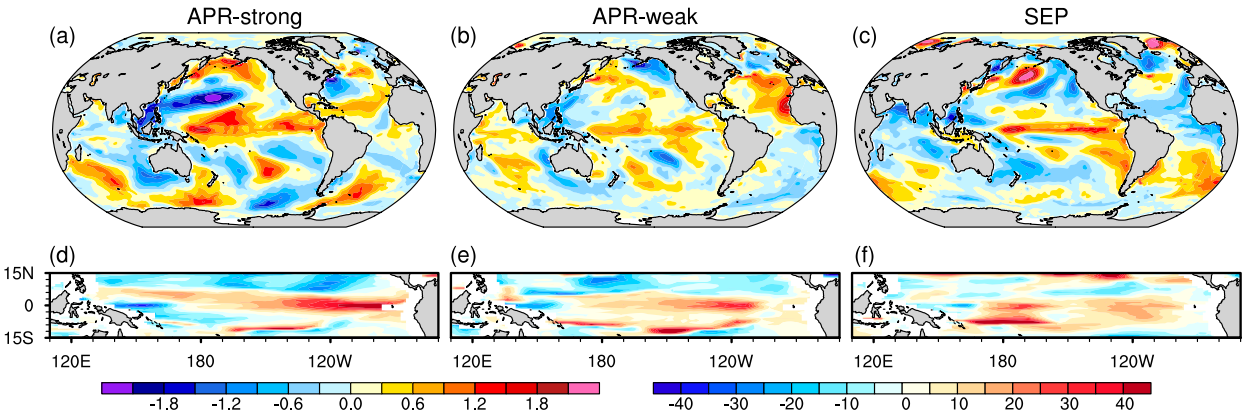

FIG. 2. Initial conditions of the (a)–(c) global SST (°C) and (d)–(f) tropical Pacific thermocline depth (m) anomalies for the (a),(d) APR-strong, (b),(e) APR-weak, and (c),(f) SEP ensembles.

($\sim 10^{-14}$) error unique to each ensemble member, which leads to a spread of weather trajectories. As noted by Kumar et al. (2001), an ensemble size of 10–20 is sufficient to estimate the predictive skills for a system with the signal-to-noise ratio of ~0.5, which is satisfied in all three ensembles (cf. Fig. 4c). We use a relatively large ensemble size of 30 to better estimate both the ensemble mean and spread, as well as the differences of these quantities among the three ensembles.

All three cases are initialized with positive SST and thermocline depth anomalies across the equatorial Pacific (Fig. 2). This oceanic state with "recharged" heat content is a well-known precursor of El Niño development (Jin 1997; Meinen and McPhaden 2000). The initial condition in April 1729 shows a stronger heat content recharge compared to April 1686 and September 1236. Therefore, we refer to these three ensembles as APR-strong, APR-weak, and SEP based on the initialization month and the magnitude of initial ocean heat recharge. As we will show in section 3, the stronger ocean heat recharge leads to stronger El Niño in the APR-strong than the APR-weak and SEP ensembles. We compare the APR and SEP ensembles to assess the role of onset timing in predicting the duration of El Niño. The long separation between the April and September onsets facilitates the comparison. The APR-strong and APR-weak ensembles are used to examine the additional influence of El Niño peak amplitude on the event duration. The role of El Niño peak amplitude is not investigated for late-onset El Niño, since the El Niño events that develop after July are consistently weak in CESM1 (not shown). The ensemble experiments conducted in this study are not affected by problems common in the operational forecasts, such as the initialization shock caused by errors in the initial conditions and the model drift resulting from biases in the model climatology, because the initial conditions are taken from the control simulation of the same model. These "perfect model predictions" allow an assessment of the maximum predictability of El Niño duration in a given model. The predictive skills in the real world would be inherently lower.

We compute oceanic and atmospheric anomalies in each member of the ensembles based on the monthly climatology of the CESM1 control simulation. We interpret the ensemble mean and spread of these anomalies as the predictable and unpredictable components of each ensemble, respectively. The ensemble spread is calculated as the standard deviation of individual members in each ensemble. The relative magnitude of the ensemble mean to the ensemble spread (i.e., signal-to-noise ratio) is used to measure the predictability. The statistical significance of the composite and correlation analyses is assessed through a two-tailed Student's t test.

3. Results

a. Predictability of El Niño duration

Nearly all members of the three prediction ensembles show the onset of El Niño in year 0, but each ensemble exhibits distinct temporal evolution in terms of the peak amplitude and event duration (Fig. 3). Both APR-strong and APR-weak ensembles show consistent termination of El Niño in year 1, albeit with a difference between the numbers of members exhibiting this transition. El Niño is predicted to terminate in all members of the APR-strong ensemble and 27 out of 30 members (90%) of the APR-weak ensemble. In the SEP ensemble, by contrast, El Niño is predicted to persist into the second year and reintensify in summer to fall in 25 out of 30 members (83%), although the Dec^{+1} Niño-3.4 index shows the largest spread among the three ensembles. The perfect model predictions successfully estimate the El Niño duration in the control simulation for all three cases with a lead time of 21 (APR-strong and APR-weak) or 16 (SEP) months. The contrast between the APR and SEP ensembles is consistent with the statistical analysis based on observations and the CESM1 control simulation (Fig. 1).

It is noted that El Niño shows a stronger tendency to transition into La Niña in the APR-strong ensemble (27 out of 30 members) relative to the APR-weak ensemble (16 out of 30 members). The consistency of La Niña states in the second winter appears to be linked to the peak amplitude of El Niño, which is on average larger in the APR-strong than the APR-weak ensemble. The larger amplitude of El Niño in the APR-strong ensemble also suggests that both early onset and large

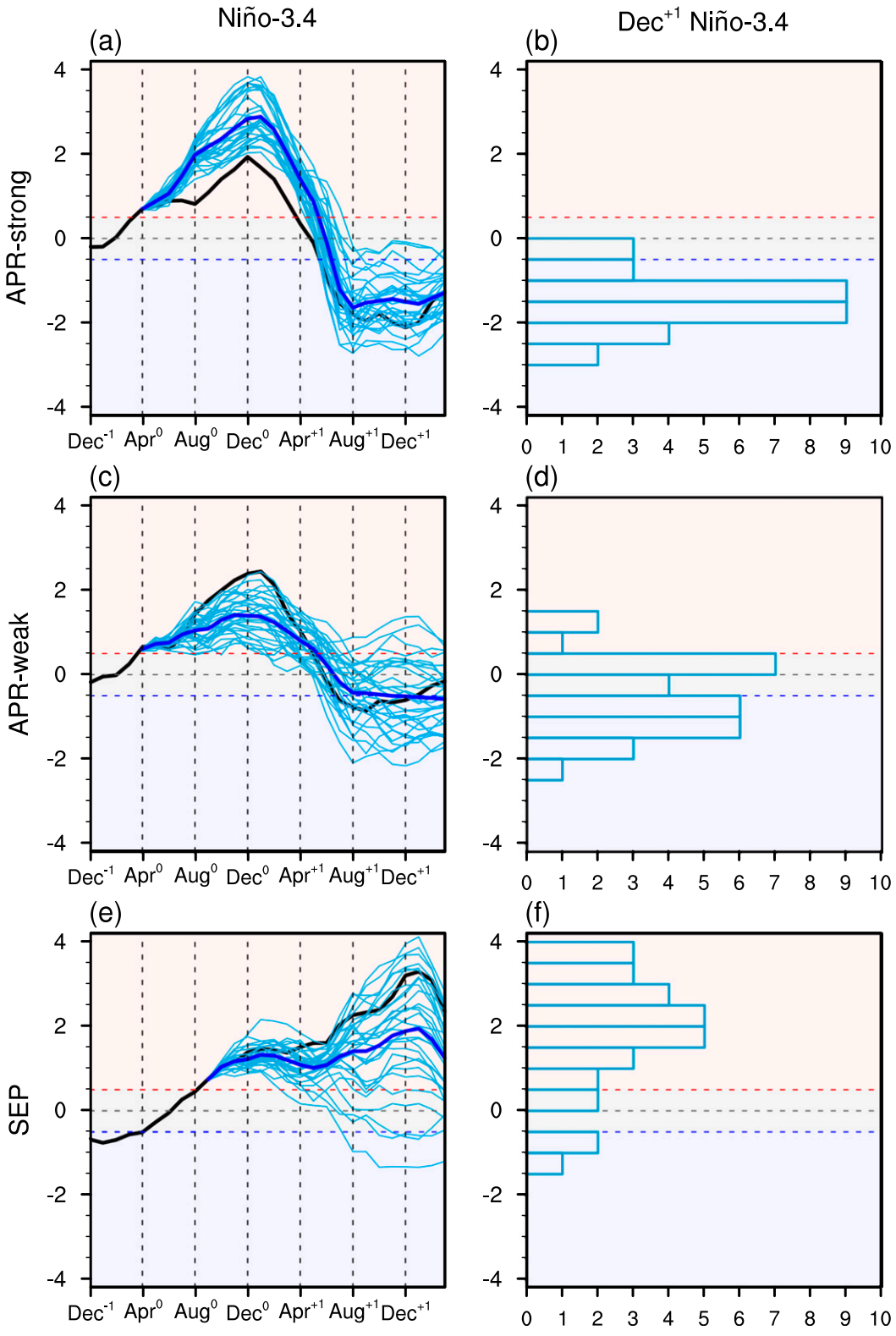

FIG. 3. (a),(c),(e) Time series of the Niño-3.4 index (°C) from the initialization month to Mar^{+2} and (b),(d),(f) histograms of the Dec^{+1} Niño-3.4 index (°C) in the (a),(b) APR-strong, (c),(d) APR-weak, and (e),(f) SEP ensembles. In (a), (c), and (e), the mean and individual members of the ensembles are indicated by thick blue and thin light blue curves, respectively. The time series of the Niño-3.4 index in the CESM1 control simulation are also shown from Dec^{-1} to Mar^{+2} by black curves.

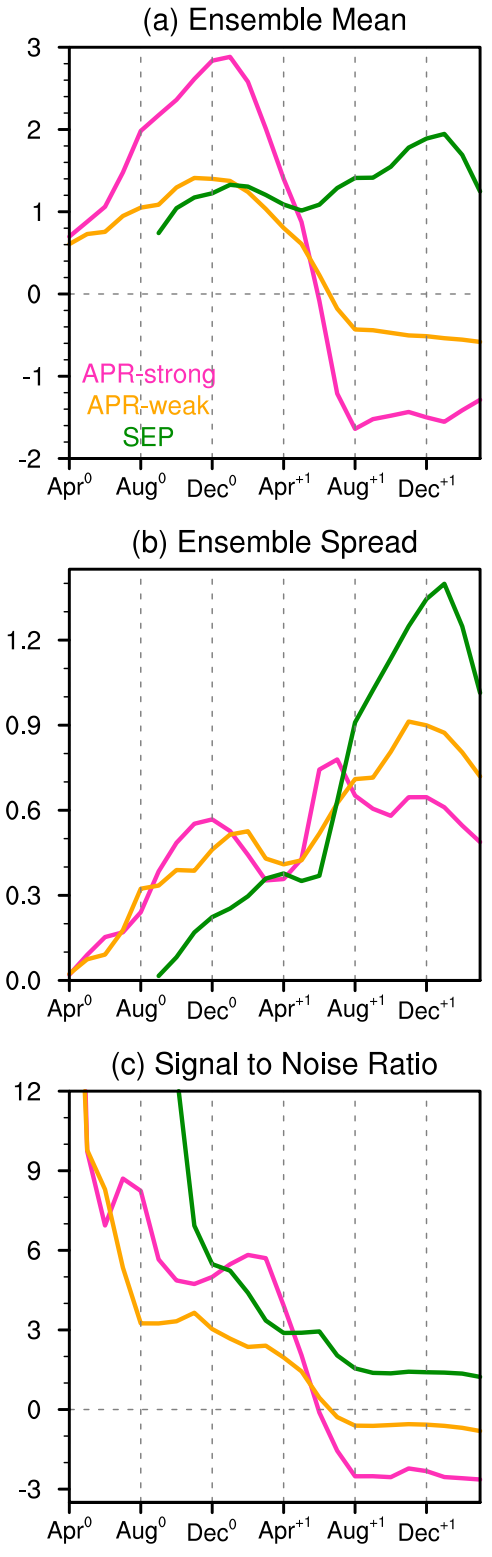

FIG. 4. Temporal evolution of the (a) ensemble mean (°C), (b) ensemble spread (°C), and (c) signal-to-noise ratio of the Niño-3.4 index from the initialization month to Mar^{+2} in the APR-strong (pink), APR-weak (orange), and SEP (green) ensembles.

initial recharge are required to develop a strong event in CESM1 (Larson and Kirtman 2019), although this is not always the case in other models (Larson and Pegion 2020). We note that the peak amplitude of El Niño simulated in the control run is outside the range of 30 ensemble members of both the APR-strong and APR-weak ensembles. This result indicates that a larger ensemble size is needed to capture the full range of predictions, or that the round-off level perturbations used to generate the ensembles may not sufficiently represent the uncertainty of atmospheric initial conditions.

The signal-to-noise ratio of the predicted Niño-3.4 index remains above 1.0 in absolute value through year 1 in the SEP ensemble and except during the ENSO phase transition in the APR-strong ensemble, indicating high predictability of El Niño duration (Fig. 4c, pink and green curves). In the APR-weak ensemble, the absolute value of signal-to-noise ratio falls below 1.0 after boreal spring of year 1 due to relatively small ensemble mean and large ensemble spread (Fig. 4c, orange curve). The ensemble spread generally grows with lead time in the three ensembles but also exhibits dependencies on the seasonal conditions and the ENSO states (Fig. 4b). For example, the ensemble spread shows a rapid growth from late spring to early summer of year 1 in all three cases, suggestive of the role of springtime atmospheric variability and subsequent ocean–atmosphere interactions during the equatorial cold season (Larson and Kirtman 2015, 2017). The ensemble spread continues to grow through the following summer to fall in the SEP ensemble (Fig. 4b; green curve) but starts to decrease in the APR-strong ensemble as negative SST anomalies develop in the equatorial Pacific (Fig. 4b; pink curve). In the following two subsections, we will examine the dynamical processes underlying the predictability and diversity of El Niño duration by analyzing the ensemble mean and spread of the perfect model predictions.

b. Processes controlling the predictability of El Niño duration

1) ENSEMBLE MEAN

To understand what controls the predictable component of El Niño duration in the perfect model predictions, we compare the ensemble mean evolution of thermocline depth, surface wind, and SST anomalies in the equatorial (3°S–3°N) and off-equatorial (6°–12°N) Pacific among the three cases (Fig. 5; see Fig. S1 in the online supplemental material for the statistical significance). The thermocline depth is estimated as the model vertical level with the maximum vertical temperature gradient. We focus on the slow oceanic adjustments to surface wind anomalies that provide negative feedback to ENSO events (Suarez and Schopf 1988; Battisti and Hirst 1989; Jin 1997). In the APR-strong and APR-weak ensembles, negative thermocline anomalies forced by positive surface wind stress curl anomalies travel westward in the off-equatorial Pacific during boreal summer-fall of year 0 (Figs. 5a,b; 6°–12°N), indicating the role of upwelling off-equatorial Rossby waves. Upon reaching the western boundary around Nov^0, the negative thermocline depth anomalies propagate equatorward as coastal Kelvin waves (Figs. 5a,b; 130°E) and then eastward as equatorial Kelvin waves, arriving at the eastern

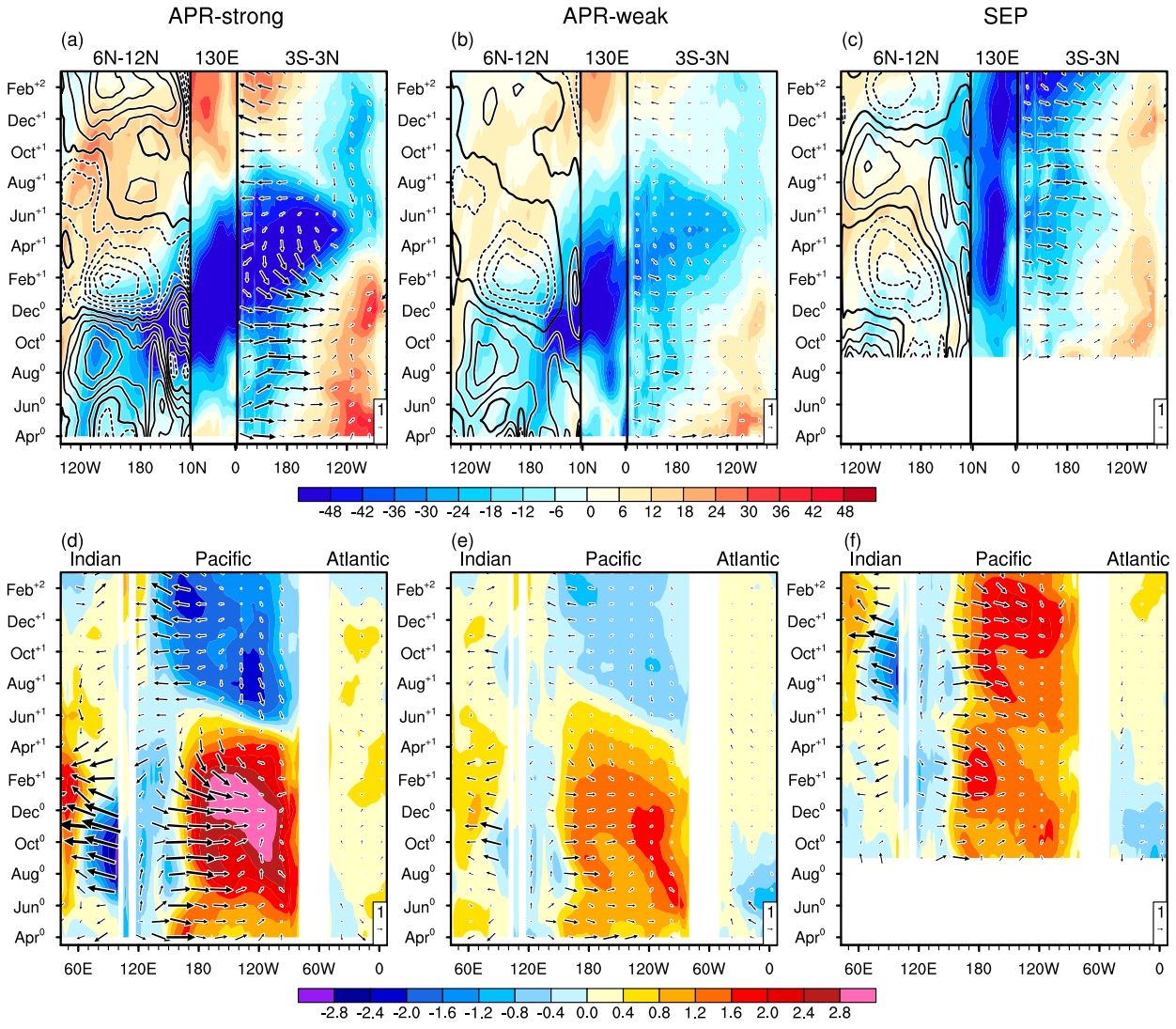

FIG. 5. (a)–(c) Longitude–latitude–time sections of the ensemble-mean thermocline depth anomalies (m; shading) along the off-equatorial Pacific (6°–12°N), western Pacific boundary (130°E), and equatorial Pacific (3°S–3°N) waveguides from the initialization month to Mar^{+2} in the (a) APR-strong, (b) APR-weak, and (c) SEP ensembles. Surface wind (m s^{-1}; vectors) and surface wind stress curl (N m^{-3}; contours at interval of 10^{-8}; zero contours thickened) anomalies are overlaid in the equatorial and off-equatorial segments, respectively. Note that the longitude axis is reversed for the off-equatorial segment to better show the Rossby wave reflection at the western boundary. (d)–(f) Longitude–time sections of the ensemble-mean SST (°C; shading) and surface wind (m s^{-1}; vectors) anomalies along the equator (3°S–3°N) from the initialization month to Mar^{+2} in the (d) APR-strong, (e) APR-weak, and (f) SEP ensembles. The statistical significance of these anomalies is shown in Fig. S1.

equatorial Pacific in Apr^{+1} (Figs. 5a,b; 3°S–3°N). The resultant reversal of thermocline depth anomalies precedes the development of negative SST anomalies in the eastern equatorial Pacific (Figs. 5d,e). These negative SST anomalies subsequently propagate westward during year 1. In the SEP ensemble, by contrast, the upwelling off-equatorial Rossby waves, which develop in late fall to winter of year 0 and are weaker than those in the APR-strong and APR-weak ensembles, do not reach the eastern equatorial Pacific before El Niño starts to redevelop in summer of year 1 (Fig. 5c). The redevelopment of El Niño SST anomalies begins in the eastern equatorial Pacific and shows subsequent westward propagation (Fig. 5f). Thus, the timing of El Niño onset appears to control the event duration by affecting the timing of negative oceanic feedback and the sign of eastern Pacific thermocline depth anomalies. The importance of the eastern Pacific thermocline in affecting the duration of El Niño events is consistent with our previous analysis (Wu et al. 2019).

Besides the reflection of off-equatorial Rossby waves, the upwelling Kelvin waves that terminate El Niño in the APR-strong and APR-weak ensembles are associated with the demise of surface westerly wind anomalies over the western equatorial Pacific after the peak (Figs. 5d,e). In the APR-strong ensemble, westerly wind anomalies are even replaced with easterly wind anomalies in the following spring (Fig. 5d).

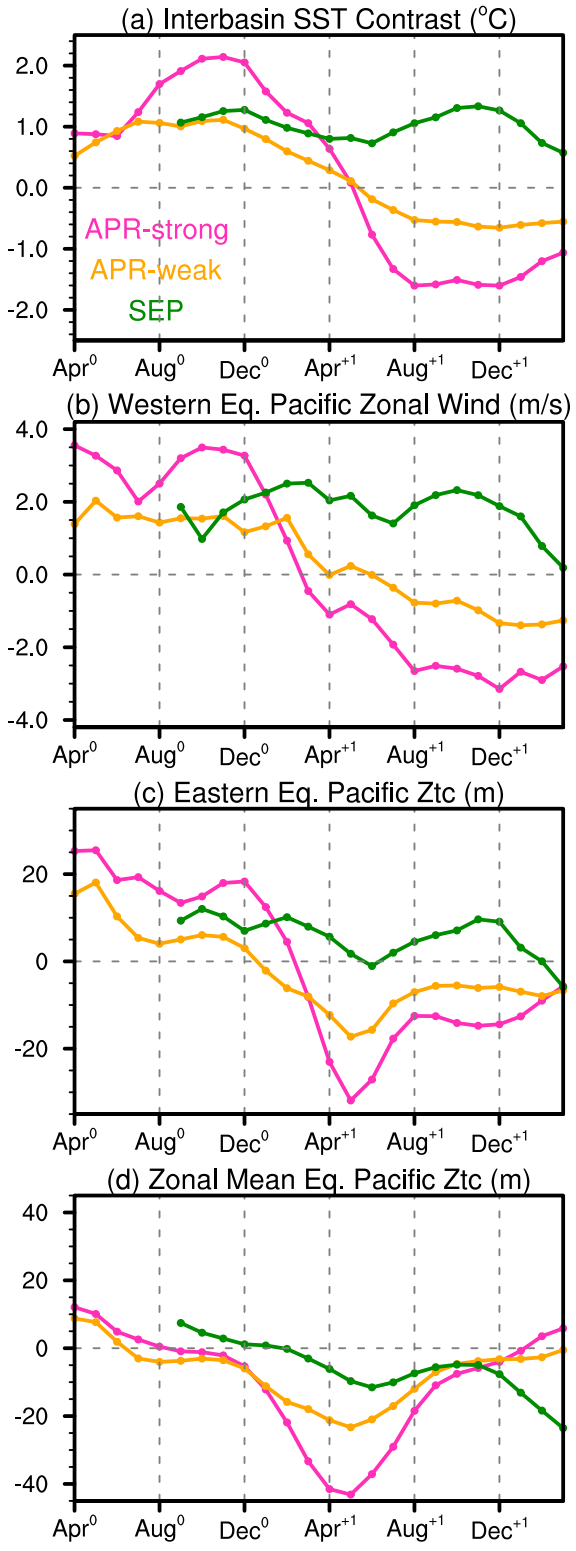

FIG. 6. Time series of the ensemble-mean ocean–atmosphere anomalies in the equatorial regions (3°S–3°N) from the initialization month to Mar^{+2} in the APR-strong (pink), APR-weak, (orange), and SEP (green) ensembles. The panels show (a) interbasin SST contrast (°C) between the Pacific and Indian/Atlantic Oceans (140°E–80°W minus 50°W–100°E), (b) surface zonal wind (m s^{-1}) over the western Pacific (130°–170°E), and thermocline depth (m) in the (c) eastern (150°–80°W) and (d) entire (140°E–80°W) Pacific.

In the SEP ensemble, in contrast, westerly wind anomalies persist through year 1 (Fig. 5f). The demise of westerly wind anomalies in the APR-strong and APR-weak ensembles could be related to basinwide SST warming over the tropical Indian and Atlantic Oceans (Figs. 5d,e). It is known that tropical Pacific warming associated with El Niño causes delayed warming of the tropical Indian and Atlantic Oceans via atmospheric teleconnections (e.g., Xie and Carton 2004; Chang et al. 2006; Schott et al. 2009). This interbasin SST adjustments, in turn, reduce anomalous SST contrast between the tropical Pacific and Indian/Atlantic Oceans and weaken westerly wind anomalies in the western equatorial Pacific (e.g., Kug and Kang 2006; Ohba and Ueda 2007; Yoo et al. 2010; Okumura et al. 2011; Ding et al. 2012; Ham and Kug 2015; Wu et al. 2019). The importance of interbasin interactions in the evolution of ENSO events has been suggested by many recent studies [see a review by Cai et al. (2019)]. The tropical Indian and Atlantic Oceans show earlier and stronger warming in the APR-strong/weak than the SEP ensemble due to the earlier onset of El Niño (Figs. 5d–f). In the APR-strong and APR-weak ensembles, the earlier onset of El Niño also results in the development of the Indian Ocean dipole (IOD) during fall of year 0, which may contribute to the stronger basin warming in the following seasons (Hong et al. 2010). In the SEP ensemble, the interbasin SST adjustments may be further delayed by initial SST cooling in the tropical Indian and Atlantic Oceans (Fig. 2c).

The anomalous SST contrast between the tropical Pacific and the tropical Indian and Atlantic Oceans starts to decrease one month before the peak of El Niño in the APR-strong/weak ensembles (Fig. 6a). Concurrently, surface westerly wind anomalies start to weaken over the western equatorial Pacific (Fig. 6b). In the SEP ensemble, interbasin SST contrast and westerly wind anomalies remain of similar magnitude after the peak of El Niño (Figs. 6a,b). Previous studies suggest that a southward shift of surface westerly wind anomalies during the mature phase of El Niño plays an important role in the event termination (Harrison and Vecchi 1999; Lengaigne et al. 2006; McGregor et al. 2012, 2013; Stuecker et al. 2013, 2015; Abellán and McGregor 2016). In all three ensembles, the center of westerly wind anomalies moves south of the equator from boreal fall to spring, following the seasonal migration of the western Pacific warm pool (not shown). The southward shift of westerly wind anomalies is particularly pronounced for the APR-strong case presumably due to the strong El Niño amplitude (Lengaigne et al. 2006; McGregor et al. 2013), which may contribute to the rapid decrease of equatorial westerly wind anomalies (Fig. 6b, pink curve). The southward wind shift may provide a favorable precondition for the Indian Ocean warming to influence the atmospheric circulation over the northwestern Pacific (Stuecker et al. 2015). The relative

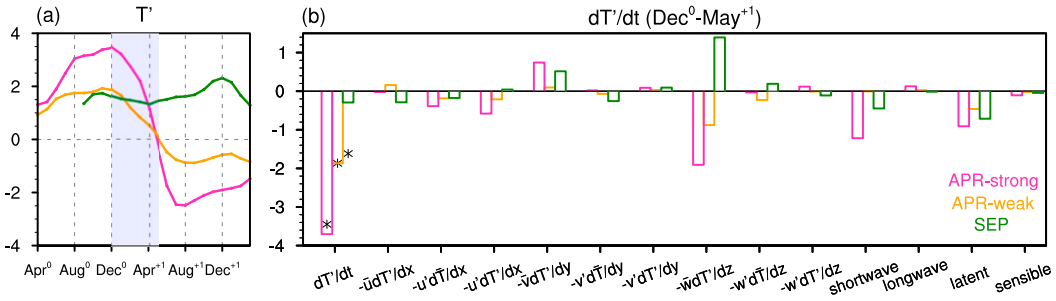

FIG. 7. (a) Time series of the ensemble-mean ocean mixed layer temperature anomalies (°C) in the eastern equatorial Pacific (3°S–3°N, 170°–120°W) and (b) ensemble-mean ocean mixed layer heat balance terms [Eq. (1)] averaged in the same region and integrated from Dec^0 to May^{+1} (°C) in the APR-strong (pink), APR-weak (orange), and SEP (green) ensembles. The black asterisks in (b) indicate the mixed layer temperature anomalies in Dec^0 with the sign reversed.

importance of interbasin SST interactions and the meridional wind shift within the Pacific in affecting the wind variability requires future examination.

The demise of westerly wind anomalies in the APR-strong and APR-weak ensembles coincides with the accelerated shoaling of the eastern equatorial Pacific thermocline, while both westerly wind and thermocline anomalies persist into the second year in the SEP ensemble (Fig. 6c). Further modeling studies are needed to understand the relative contributions of the wind change and upwelling Rossby wave reflection to this rapid thermocline shoaling. It is noted that all three ensembles show a gradual shoaling of the eastern equatorial Pacific thermocline after the onset of El Niño, indicating the role of slow oceanic adjustments through Sverdrup transport (Jin 1997). This feature is more evident in the temporal evolution of zonal mean thermocline depth anomalies (Fig. 6d). The zonal mean thermocline depth, however, is not a good precursor of the El Niño duration, as it turns negative in year 1 for all three cases. The slow oceanic adjustments are not sufficient to reverse the thermocline depth anomalies in the eastern Pacific and to terminate El Niño in the SEP ensemble.

To examine the role of eastern equatorial Pacific thermocline depth anomalies in affecting the El Niño duration, we conduct an ocean mixed layer heat budget analysis of the ensemble mean predictions. The heat budget is computed at each horizontal grid point of the eastern equatorial Pacific as a balance among the heat storage tendency, oceanic temperature advection, and surface heat fluxes according to the following equation:

$$\frac{\partial\langle T'\rangle}{\partial t} = \left\langle -u'\frac{\partial\overline{T}}{\partial x}\right\rangle + \left\langle -\overline{u}\frac{\partial T'}{\partial x}\right\rangle + -\left\langle u'\frac{\partial T'}{\partial x}\right\rangle + \left\langle -v'\frac{\partial\overline{T}}{\partial y}\right\rangle + \left\langle -\overline{v}\frac{\partial T'}{\partial y}\right\rangle + \left\langle -v'\frac{\partial T'}{\partial y}\right\rangle + \left\langle -w'\frac{\partial\overline{T}}{\partial z}\right\rangle + \left\langle -\overline{w}\frac{\partial T'}{\partial z}\right\rangle + \left\langle -w'\frac{\partial T'}{\partial z}\right\rangle + \frac{Q'_{\text{net}}}{\rho C_p H} + R, \quad \text{where } \langle * \rangle = \frac{1}{H}\int_{-H}^{0} * dz \tag{1}$$

where T is the mixed layer temperature; u, v, and w are the zonal, meridional, and vertical ocean currents, respectively; Q_{net} is the net surface heat flux comprised of shortwave, longwave, latent, and sensible heat fluxes; ρ is the ocean water density ($10^3\,\text{kg m}^{-3}$); C_p is the ocean heat capacity ($4000\,\text{J kg}^{-1}\,\text{K}^{-1}$); H is the climatological mixed layer depth as a function of longitude based on the CESM1 control simulation; R represents the residual term; and the overbar and prime denote the climatology and anomaly, respectively.

The individual terms of Eq. (1) are averaged over the eastern equatorial Pacific (3°S–3°N, 150°–80°W) and integrated through the decay phase of El Niño (Dec^0–May^{+1}) for each ensemble mean prediction (Fig. 7). The result shows that the vertical advection of temperature anomalies by climatological upwelling ($-\overline{w}\partial T'/\partial z$; i.e., the thermocline feedback) is the main cause of different evolution of ocean mixed layer temperature anomalies between the APR and SEP ensembles. The vertical temperature gradient anomalies ($\partial T'/\partial z$) are closely related to the local thermocline depth anomalies, confirming their importance in determining the duration of El Niño. The climatological upwelling ($\overline{w}$) is strongest in boreal winter to early spring in the eastern equatorial Pacific (not shown), and thus the reversal of thermocline depth anomalies during this season can effectively affect the ocean mixed layer temperature in the APR-strong and APR-weak ensembles. In the SEP ensemble, in contrast, the thermocline depth remains positive and the thermocline feedback acts to prolong El Niño. The subsequent westward propagation of SST anomalies after the decay phase (Fig. 5) is mainly caused by the anomalous zonal advection of climatological temperature ($-u'\partial\overline{T}/\partial x$; not shown).

2) ENSEMBLE SPREAD

Now we investigate the oceanic and atmospheric processes contributing to the growth of ensemble spread in the perfect model predictions. The ensemble spread of SST anomalies in the three equatorial oceans exhibits strong seasonality similar to the seasonality of the ensemble-mean anomalies (cf. shading and contours in Figs. 8a–c), suggesting that the evolution of the ensemble mean and spread is affected by similar ocean–atmosphere feedback mechanisms. The ensemble spread of equatorial Pacific SST anomalies grows during boreal summer to fall, when the Bjerknes feedback is stronger due to the seasonal development of the equatorial cold tongue (e.g., Neelin et al. 1998). The ensemble spread of equatorial Indian Oceanic SST anomalies tends to increase during fall in the east

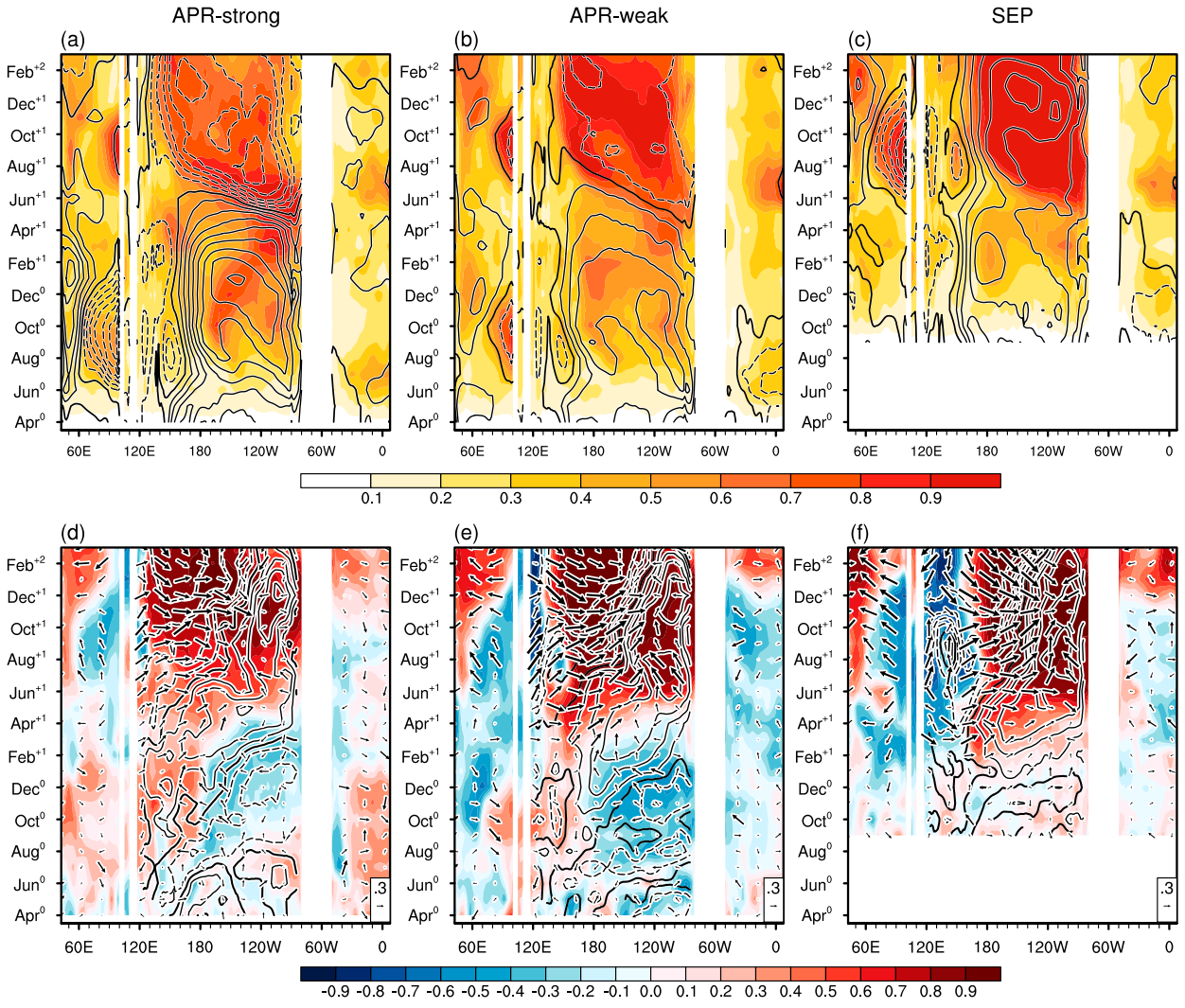

FIG. 8. (a)–(c) Longitude–time sections of the ensemble mean (contours) and spread (shading) of SST anomalies (°C) along the equator (3°S–3°N) from the initialization month to Mar^{+2} in the (a) APR-strong, (b) APR-weak, and (c) SEP ensembles. The contour interval is 0.4°C. (d)–(f) Lead–lag correlations of the Dec^{+1} Niño-3.4 index with SST (shading), surface wind (vectors), and thermocline depth (contours at intervals of 0.2) anomalies along the equator (3°S–3°N) from the initialization month to Mar^{+2} across the 30 ensemble members of the (d) APR-strong, (e) APR-weak, and (f) SEP ensembles. The statistical significance of these anomalies is shown in Fig. S2.

and during winter in the west, indicative of the role of IOD variability and associated oceanic adjustments (e.g., Xie et al. 2009; Schott et al. 2009). The ensemble spread of equatorial Atlantic SST anomalies is pronounced in summer, when Atlantic Niño, an equatorial mode analogous to the ENSO, is most active (e.g., Zebiak 1993; Xie and Carton 2004).

To understand how the ensemble spread of ocean–atmosphere anomalies in the three tropical oceans affects the duration of El Niño events, we correlate the Dec^{+1} Niño-3.4 index with SST, thermocline depth, and surface wind anomalies along the equator from Apr^{0} to Mar^{+2} across individual ensemble members for each ensemble (Figs. 8d–f; see Fig. S2 for the statistical significance). In all three cases, positive zonal wind correlations emerge over the western Pacific around Mar^{+1}, followed by zonal propagation of positive thermocline correlations and development of positive SST correlations in the Pacific. This result indicates that western Pacific wind variability during spring after the El Niño peak plays an important role in affecting the eastern Pacific thermocline depth and hence the event duration. These positive zonal wind correlations are, in turn, associated with negative SST correlations in the Indian and Atlantic Oceans, although the correlations are not statistically significant along the equator. More significant SST correlations are found in the northern tropical Indian Ocean and the tropical South Atlantic (cf. Fig. 10 and Fig. S3). The wind and thermocline correlations are weaker in the APR-strong ensemble compared to the other two cases, indicating a reduced sensitivity of the El Niño evolution to wind variability. Note that El Niño terminates in all members of the APR-strong ensemble and thus the Dec^{+1} Niño-3.4 index simply represents the amplitude of ensuing La Niña. In the APR-strong and APR-weak ensembles,

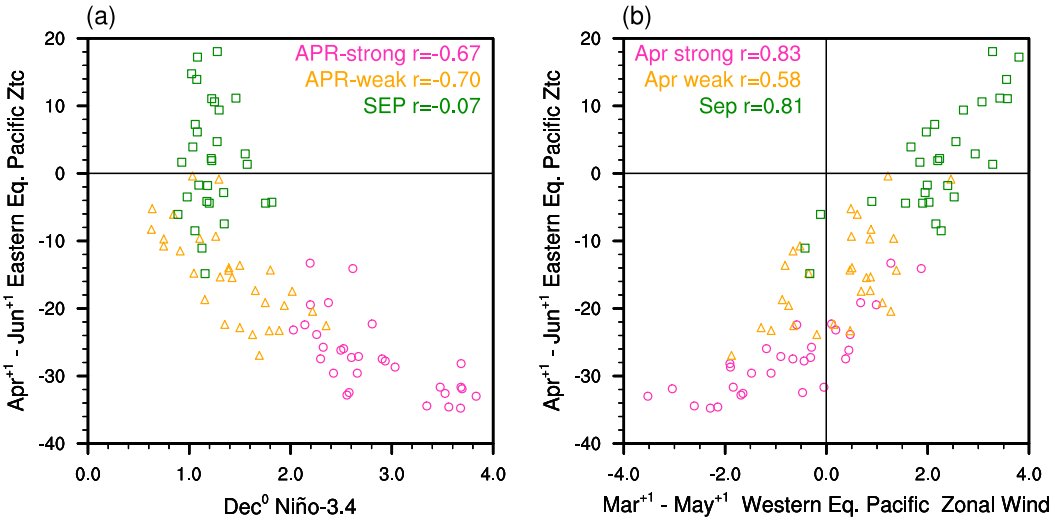

FIG. 9. Scatterplots of Apr^{+1}–Jun^{+1} thermocline depth anomalies in the eastern equatorial Pacific (3°S–3°N; 150°–80°W) vs (a) the Dec^{0} Niño-3.4 index and (b) Mar^{+1}–May^{+1} surface zonal wind anomalies over the western equatorial Pacific (3°S–3°N; 130°–170°E) in the APR-strong (pink), APR-weak (orange), and SEP (green) ensembles. The numbers near the top of each panel indicate the correlation coefficients for the three ensembles.

SST and thermocline depth also show weak negative correlations in the eastern Pacific around the peak of El Niño (Dec^{0}–Jan^{+1}). This result suggests that variations in the amplitude of El Niño have an additional impact on the event duration by affecting the magnitude of negative oceanic feedback and interbasin SST adjustments.

The impacts of El Niño amplitude and western Pacific wind variability on the eastern Pacific thermocline depth are further assessed in Fig. 9. In the APR-strong and APR-weak ensembles, the eastern Pacific thermocline depth in Apr^{+1}–Jun^{+1} is highly correlated with both the Niño-3.4 index in Dec^{0} (r = 0.67–0.70) and western Pacific zonal wind in Mar^{+1}–May^{+1} (r = 0.58–0.83). However, neither the El Niño amplitude nor western Pacific wind variability affects the sign of thermocline depth anomalies in the eastern Pacific because of large thermocline shoaling in the ensemble mean. This is particularly true in the APR-strong ensemble, explaining the small ensemble spread of El Niño duration. In the SEP ensemble, the eastern Pacific thermocline depth in Apr^{+1}–Jun^{+1} is significantly correlated only with western Pacific zonal wind in Mar^{+1}–May^{+1} (r = 0.81). Due to the late onset of El Niño in these ensemble simulations, the negative feedbacks do not set in by boreal spring, and western Pacific wind variability in Mar^{+1}–May^{+1} can easily affect the sign of eastern Pacific thermocline depth anomalies in Apr^{+1}–Jun^{+1}. The resultant ensemble spread of thermocline depth anomalies are further amplified in the subsequent seasons due to the Bjerknes feedback, leading to the large ensemble spread of El Niño duration.

To understand the origins of wind variability, we correlate surface zonal wind anomalies averaged over the western 2equatorial Pacific in Mar^{+1}–May^{+1} with global SST, surface wind, precipitation, and sea level pressure (SLP) anomalies in the same season and Dec^{0}–Feb^{+1} across individual ensemble members (Fig. 10; see Fig. S3 for the statistical significance). For this analysis, all 90 members of the three ensembles are combined after removing the mean of each ensemble from individual members to increase the sample size. In Mar^{+1}–May^{+1}, the wind index is correlated positively with SST and precipitation over the western tropical Pacific and negatively with SST over the northern tropical Indian Ocean and the tropical South Atlantic, indicating the role of interbasin teleconnections as discussed earlier. The SST correlations in the northwestern tropical Pacific also display a meridional dipole pattern reminiscent of the North Pacific meridional mode (NPMM; e.g., Anderson 2003; Vimont et al. 2003; Chang et al. 2007; Alexander et al. 2010). Indeed, SLP correlations in Dec^{0}–Feb^{+1} show a meridional dipole pattern over the North Pacific similar to the North Pacific Oscillation (NPO), which is known to drive the NPMM in the following spring through thermodynamic air–sea interactions and affect ENSO events [see Amaya (2019) for a recent review]. Thus, ocean–atmosphere variability not only in the tropics but also in the North Pacific appears to have an impact on the duration of El Niño by affecting surface winds over the western equatorial Pacific. The role of NPMM in causing the ensemble spread of ENSO predictions is consistent with a previous study (Ma et al. 2017). It should be noted, however, that these NPO circulation anomalies may be partly forced by tropical Pacific SST anomalies (Wu et al. 2019). In Dec^{0}–Feb^{+1}, tropical Pacific SST correlations show a zonal dipole pattern, suggesting that diversity in the pattern of El Niño warming may affect the event duration by shifting the pattern of westerly wind anomalies. Further model experiments are needed to understand the relative importance of different processes that affect the ensemble spread of wind variability.

4. Summary and discussion

We explored the predictability of El Niño duration based on the onset timing using perfect model experiments performed

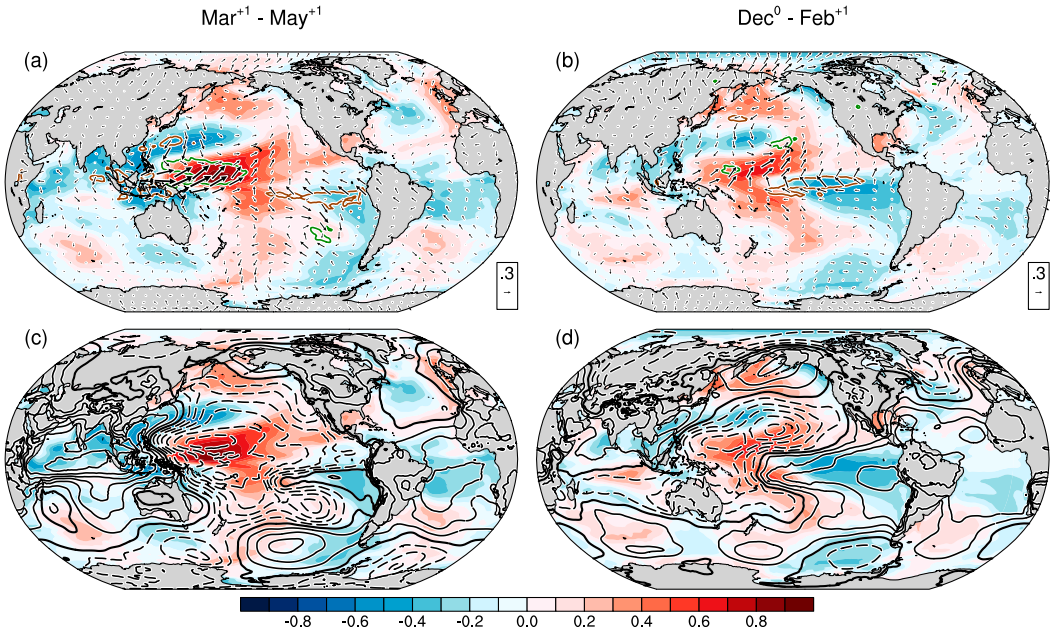

FIG. 10. Global correlation maps based on Mar^{+1}–May^{+1} surface zonal wind anomalies averaged over the western equatorial Pacific (3°S–3°N, 130°–170°E). The correlations are calculated with (a),(b) SST (shading), surface wind (vectors), and rainfall anomalies [positive (negative) contours in green (brown) at intervals of 0.4) and (c),(d) SST (shading) and SLP (contours at intervals of 0.1; zero contours thickened) anomalies in (a),(c) Mar^{+1}–May^{+1} and (b),(d) Dec^{0}–Feb^{+1} across individual ensemble members. All 90 members of the three ensembles are used after removing the mean of each ensemble from individual members. The statistical significance of these correlations is shown in Fig. S3.

with CESM1, a climate model that reproduces the observed dependency of El Niño duration on the onset timing. The CESM1 successfully predicts the duration of El Niño events when initialized with the oceanic, land, and sea ice conditions in their onset months. In two ensembles initialized in April, El Niño consistently terminates after peaking in boreal winter. In the ensemble initialized in September, El Niño on average persists into the second year and reintensifies in boreal winter, although the ensemble spread is larger than that in the April-initialized ensembles. The signal-to-noise ratio of the predicted Niño-3.4 SST index remains larger than one at the end of the second year except in one April-initialized ensemble, indicating high predictability with lead times up to 16–21 months. The predictability of El Niño duration arises from the oceanic initial conditions in the equatorial Pacific, particularly the timing and magnitude of thermocline depth anomalies in the onset month. The early onset of El Niño leads to early arrival of negative oceanic feedback in the equatorial Pacific and early adjustment of remote tropical oceans, which together act to shoal the thermocline in the eastern equatorial Pacific and terminate El Niño after the peak. The late onset of El Niño delays the onset of these negative feedbacks, and El Niño starts to redevelop in summer of the second year while the eastern Pacific thermocline remains deeper than normal. Our results suggest that the effectiveness of delayed oceanic feedback in terminating El Niño depends on the timing of arrival relative to the seasonal cycle of the equatorial Pacific.

In the April-initialized ensembles, the eastern equatorial Pacific thermocline consistently shoals during spring following the peak due to the early occurrence of negative feedbacks, leading to a consistent termination of El Niño. Furthermore, when early-onset El Niño develops into a strong event due to a large initial recharge of the oceanic heat content, the attendant large thermocline shoaling makes the ocean–atmosphere coupled system consistently transition into a La Niña state in the second year. In the September-initialized ensemble, on the other hand, the eastern Pacific thermocline depth is strongly affected by surface wind variability over the western equatorial Pacific after the El Niño peak due to the delay in negative feedbacks, resulting in a large ensemble spread of the event duration. The western Pacific wind variability can be affected by SST variability in the tropical Indian/Atlantic Oceans and the NPMM, as well as diversity in the pattern of El Niño warming within the tropical Pacific Ocean.

The importance of oceanic initial conditions in the equatorial Pacific for the predictability of El Niño duration is consistent with earlier studies of the predictability of other ENSO properties, including the event onset and amplitude (Wyrtki 1985; Meinen and McPhaden 2000; Planton et al. 2018; Larson and Kirtman 2019). Our study indicates that the oceanic initial conditions in the equatorial Pacific can provide predictability of El Niño beyond the current operational ENSO forecasts. Our findings also suggest the importance of initial conditions in the tropical Indian and

Atlantic Oceans, in predicting El Niño duration. For example, in the September-initialized ensemble, the initial SST cooling of the tropical Indian and Atlantic Oceans may contribute to the persistency of El Niño by delaying the interbasin SST adjustments. Many recent studies suggest that the predictions of the amplitude, pattern, and evolution of ENSO events can be improved with information outside the tropical Pacific (Luo et al. 2010; Izumo et al. 2010; Lim and Hendon 2017; Frauen and Dommenget 2012; Dayan et al. 2014; Keenlyside et al. 2013; Martín-Rey et al. 2015; Ohba and Watanabe 2012; Luo et al. 2017; Larson and Kirtman 2014; You and Furtado 2017). Further studies are needed in the future to understand the relative importance of oceanic initial conditions in different ocean basins for the predictability of El Niño duration. Improving our understanding of the interbasin linkages, as well as realistic representation of these processes in climate models, is key to improve ENSO predictions.

The results of the CESM1 perfect model experiments agree with our previous diagnostic study based on a suite of observational datasets and a control simulation of the same model (Wu et al. 2019). However, due to the limited number of prediction ensembles and the use of a single climate model, it remains to be seen to what degree the results apply to other El Niño events and climate models. In particular, it is important to understand how the variations in initial oceanic conditions within and outside the tropical Pacific affect the predictability of El Niño duration for individual events. The multiyear predictability should also be tested with other climate models. Larson and Pegion (2020) show that climate models tend to underestimate the uncertainty of ENSO variability in nature and the problem could be exacerbated in predictions based on a single model. Due to the potential problem in the ensemble generation method noted earlier, the predictability is likely overestimated in our experiments.

Despite the caveats discussed above, the results presented in this study and the recent advance in predicting multiyear La Niña events (DiNezio et al. 2017a,b; Luo et al. 2017) indicate the potential to extend the operational ENSO forecasts by an additional year. Future studies are needed to explore the predictability of both El Niño and La Niña duration in the real world based on forecasts initialized with observed oceanic conditions using the CESM1 and other state-of-the-art climate models. Predicting the occurrence of multiyear ENSO events with sufficient lead times would benefit our society due to their lingering climate impacts.

Acknowledgments. The authors thank Dr. Martin Puy for helpful discussions and Dr. Sarah Larson and two anonymous reviewers for helpful comments and suggestions. The CESM1 control simulation is conducted by the CESM project team and available via the Earth System Grid (https://www.earthsystemgrid.org). The HadISST dataset used in this study is obtained online from the Met Office Hadley Center (http://www.metoffice.gov.uk/hadobs/). This study is supported by the NOAA Climate Program Office Modeling, Analysis, Predictions, and Projections Program (NA17OAR4310149 and NA17OAR4310145) and the NSF Physical Oceanography Program (OCE-1756883).

REFERENCES

Abellán, E., and S. McGregor, 2016: The role of the southward wind shift in both the seasonal synchronization and duration of ENSO events. *Climate Dyn.*, **47**, 509–527, https://doi.org/10.1007/s00382-015-2853-1.

Alexander, M. A., I. Bladé, M. Newman, J. R. Lanzante, N.-C. Lau, and J. D. Scott, 2002: The atmospheric bridge: The influence of ENSO teleconnections on air–sea interaction over the global oceans. *J. Climate*, **15**, 2205–2231, https://doi.org/10.1175/1520-0442(2002)015<2205:TABTIO>2.0.CO;2.

——, D. J. Vimont, P. Chang, and J. D. Scott, 2010: The impact of extratropical atmospheric variability on ENSO: Testing the seasonal footprinting mechanism using coupled model experiments. *J. Climate*, **23**, 2885–2901, https://doi.org/10.1175/2010JCLI3205.1.

Amaya, D. J., 2019: The Pacific meridional mode and ENSO: A review. *Curr. Climate Change Rep.*, **5**, 296–307, https://doi.org/10.1007/s40641-019-00142-x.

Anderson, B. T., 2003: Tropical Pacific sea-surface temperatures and preceding sea level pressure anomalies in the subtropical North Pacific. *J. Geophys. Res.*, **108**, 4732, https://doi.org/10.1029/2003JD003805.

Barnston, A. G., M. K. Tippett, M. L. L'Heureux, S. Li, and D. G. DeWitt, 2012: Skill of real-time seasonal ENSO model predictions during 2002–11: Is our capability increasing? *Bull. Amer. Meteor. Soc.*, **93**, 631–651, https://doi.org/10.1175/BAMS-D-11-00111.1.

——, ——, M. Ranganathan, and M. L. L'Heureux, 2019: Deterministic skill of ENSO predictions from the North American multimodel ensemble. *Climate Dyn.*, **53**, 7215–7234, https://doi.org/10.1007/s00382-017-3603-3.

Battisti, D. S., and A. C. Hirst, 1989: Interannual variability in a tropical atmosphere–ocean model: Influence of the basic state, ocean geometry and nonlinearity. *J. Atmos. Sci.*, **46**, 1687–1712, https://doi.org/10.1175/1520-0469(1989)046<1687:IVIATA>2.0.CO;2.

Cai, W., and Coauthors, 2019: Pantropical climate interactions. *Science*, **363**, eaav4236, https://doi.org/10.1126/science.aav4236.

Capotondi, A., and Coauthors, 2015: Understanding ENSO diversity. *Bull. Amer. Meteor. Soc.*, **96**, 921–938, https://doi.org/10.1175/BAMS-D-13-00117.1.

Chang, P., and Coauthors, 2006: Climate fluctuations of tropical coupled systems—The role of ocean dynamics. *J. Climate*, **19**, 5122–5174, https://doi.org/10.1175/JCLI3903.1.

——, L. Zhang, R. Saravanan, D. J. Vimont, J. C. H. Chiang, L. Ji, H. Seidel, and M. K. Tippett, 2007: Pacific meridional mode and El Niño–Southern Oscillation. *Geophys. Res. Lett.*, **34**, L16608, https://doi.org/10.1029/2007GL030302.

Chen, D., and M. A. Cane, 2008: El Niño prediction and predictability. *J. Comput. Phys.*, **227**, 3625–3640, https://doi.org/10.1016/j.jcp.2007.05.014.

Dayan, H., J. Vialard, T. Izumo, and M. Lengaigne, 2014: Does sea surface temperature outside the tropical Pacific contribute to enhanced ENSO predictability? *Climate Dyn.*, **43**, 1311–1325, https://doi.org/10.1007/s00382-013-1946-y.

DiNezio, P. N., and C. Deser, 2014: Nonlinear controls on the persistence of La Niña. *J. Climate*, **27**, 7335–7355, https://doi.org/10.1175/JCLI-D-14-00033.1.

——, ——, Y. M. Okumura, and A. Karspeck, 2017a: Predictability of 2-year La Niña events in a coupled general circulation model. *Climate Dyn.*, **49**, 4237–4261, https://doi.org/10.1007/s00382-017-3575-3.

——, and Coauthors, 2017b: A 2 year forecast for a 60–80% chance of La Niña in 2017–2018. *Geophys. Res. Lett.*, **44**, 11 624–11 635, https://doi.org/10.1002/2017GL074904.

Ding, H., N. S. Keenlyside, and M. Latif, 2012: Impact of the equatorial Atlantic on the El Niño Southern Oscillation. *Climate Dyn.*, **38**, 1965–1972, https://doi.org/10.1007/s00382-011-1097-y.

Frauen, C., and D. Dommenget, 2012: Influences of the tropical Indian and Atlantic Oceans on the predictability of ENSO. *Geophys. Res. Lett.*, **39**, L02706, https://doi.org/10.1029/2011GL050520.

Ham, Y.-G., and J.-S. Kug, 2015: Role of north tropical Atlantic SST on the ENSO simulated using CMIP3 and CMIP5 models. *Climate Dyn.*, **45**, 3103–3117, https://doi.org/10.1007/s00382-015-2527-z.

Harrison, D. E., and G. A. Vecchi, 1999: On the termination of El Niño. *Geophys. Res. Lett.*, **26**, 1593–1596, https://doi.org/10.1029/1999GL900316.

Hoerling, M. P., and A. Kumar, 2002: Atmospheric response patterns associated with tropical forcing. *J. Climate*, **15**, 2184–2203, https://doi.org/10.1175/1520-0442(2002)015<2184:ARPAWT>2.0.CO;2.

Hong, C.-C., T. Li, LinHo, and Y.-C. Chen, 2010: Asymmetry of the Indian Ocean basinwide SST anomalies: Roles of ENSO and IOD. *J. Climate*, **23**, 3563–3576, https://doi.org/10.1175/2010JCLI3320.1.

Horii, T., and K. Hanawa, 2004: A relationship between timing of El Niño onset and subsequent evolution. *Geophys. Res. Lett.*, **31**, L06304, https://doi.org/10.1029/2003GL019239.

Hurrell, J., and Coauthors, 2013: The Community Earth System Model: A framework for collaborative research. *Bull. Amer. Meteor. Soc.*, **94**, 1339–1360, https://doi.org/10.1175/BAMS-D-12-00121.1.

Izumo, T., and Coauthors, 2010: Influence of the state of the Indian Ocean dipole on the following year's El Niño. *Nat. Geosci.*, **3**, 168–172, https://doi.org/10.1038/ngeo760.

Jin, E. K., and Coauthors, 2008: Current status of ENSO prediction skill in coupled ocean–atmosphere models. *Climate Dyn.*, **31**, 647–664, https://doi.org/10.1007/s00382-008-0397-3.

Jin, F.-F., 1997: An equatorial ocean recharge paradigm for ENSO. Part I: Conceptual model. *J. Atmos. Sci.*, **54**, 811–829, https://doi.org/10.1175/1520-0469(1997)054<0811:AEORPF>2.0.CO;2.

Kay, J. E., and Coauthors, 2015: The Community Earth System Model (CESM) Large Ensemble project: A community resource for studying climate change in the presence of internal climate variability. *Bull. Amer. Meteor. Soc.*, **96**, 1333–1349, https://doi.org/10.1175/BAMS-D-13-00255.1.

Keenlyside, N. S., H. Ding, and M. Latif, 2013: Potential of equatorial Atlantic variability to enhance El Niño prediction. *Geophys. Res. Lett.*, **40**, 2278–2283, https://doi.org/10.1002/grl.50362.

Kessler, W. S., 2002: Is ENSO a cycle or a series of events? *Geophys. Res. Lett.*, **29**, 2125, https://doi.org/10.1029/2002GL015924.

Kirtman, B. P., J. Shukla, M. Balmaseda, N. Graham, C. Penland, Y. Xue, and S. Zebiak, 2002: Current status of ENSO forecast skill: A report to the CLIVAR Working Group on Seasonal to Interannual Prediction. International CLIVAR Project Office Rep. 56, 24 pp.

Kug, J.-S., and I.-S. Kang, 2006: Interactive feedback between ENSO and the Indian Ocean. *J. Climate*, **19**, 1784–1801, https://doi.org/10.1175/JCLI3660.1.

Kumar, A., and M. P. Hoerling, 2000: Analysis of a conceptual model of seasonal climate variability and implications for seasonal prediction. *Bull. Amer. Meteor. Soc.*, **81**, 255–264, https://doi.org/10.1175/1520-0477(2000)081<0255:AOACMO>2.3.CO;2.

——, A. G. Barnston, and M. P. Hoerling, 2001: Seasonal predictions, probabilistic verifications, and ensemble size. *J. Climate*, **14**, 1671–1676, https://doi.org/10.1175/1520-0442(2001)014<1671:SPPVAE>2.0.CO;2.

——, B. Jha, and H. Wang, 2014: Attribution of SST variability in global oceans and the role of ENSO. *Climate Dyn.*, **43**, 209–220, https://doi.org/10.1007/s00382-013-1865-y.

Larkin, N. K., and D. E. Harrison, 2002: ENSO warm (El Niño) and cold (La Niña) event life cycles: Ocean surface anomaly patterns, their symmetries, asymmetries, and implications. *J. Climate*, **15**, 1118–1140, https://doi.org/10.1175/1520-0442(2002)015<1118:EWENOA>2.0.CO;2.

Larson, S. M., and B. P. Kirtman, 2014: The Pacific meridional mode as an ENSO precursor and predictor in the North American Multimodel Ensemble. *J. Climate*, **27**, 7018–7032, https://doi.org/10.1175/JCLI-D-14-00055.1.

——, and ——, 2015: Revisiting ENSO coupled instability theory and SST error growth in a fully coupled model. *J. Climate*, **28**, 4724–4742, https://doi.org/10.1175/JCLI-D-14-00731.1.

——, and ——, 2017: Drivers of coupled model ENSO error dynamics and the spring predictability barrier. *Climate Dyn.*, **48**, 3631–3644, https://doi.org/10.1007/s00382-016-3290-5.

——, and ——, 2019: Linking preconditioning to extreme ENSO events and reduced ensemble spread. *Climate Dyn.*, **52**, 7417–7433, https://doi.org/10.1007/s00382-017-3791-x.

——, and K. Pegion, 2020: Do asymmetries in ENSO predictability arise from different recharged states? *Climate Dyn.*, **54**, 1507–1522, https://doi.org/10.1007/s00382-019-05069-5.

Latif, M., and Coauthors, 1998: A review of the predictability and prediction of ENSO. *J. Geophys. Res.*, **103**, 14 375–14 393, https://doi.org/10.1029/97JC03413.

Lee, S.-K., P. N. DiNezio, E.-S. Chung, S.-W. Yeh, A. T. Wittenberg, and C. Wang, 2014: Spring persistence, transition and resurgence of El Niño. *Geophys. Res. Lett.*, **41**, 8578–8585, https://doi.org/10.1002/2014GL062484.

Lengaigne, M., J.-P. Boulanger, C. Menkes, and H. Spencer, 2006: Influence of the seasonal cycle on the termination of El Niño events in a coupled general circulation model. *J. Climate*, **19**, 1850–1868, https://doi.org/10.1175/JCLI3706.1.

L'Heureux, M. L., M. K. Tippett, and A. G. Barnston, 2015: Characterizing ENSO coupled variability and its impact on North American seasonal precipitation and temperature. *J. Climate*, **28**, 4231–4245, https://doi.org/10.1175/JCLI-D-14-00508.1.

——, A. F. Z. Levine, M. Newman, C. Ganter, J.-J. Luo, M. K. Tippett, and T. N. Stockdale, 2020: ENSO prediction. *El Niño Southern Oscillation in a Changing Climate*, *Geophys. Monogr.*, Vol. 253, Amer. Geophys. Union, 227–248.

Lim, E.-P., and H. H. Hendon, 2017: Causes and predictability of the negative Indian Ocean dipole and its impact on La Niña during 2016. *Sci. Rep.*, **7**, 12619, https://doi.org/10.1038/s41598-017-12674-z.

Luo, J.-J., R. Zhang, S. K. Behera, Y. Masumoto, F.-F. Jin, R. Lukas, and T. Yamagata, 2010: Interaction between El Niño and extreme Indian Ocean dipole. *J. Climate*, **23**, 726–742, https://doi.org/10.1175/2009JCLI3104.1.

——, G. Liu, H. Hendon, O. Alves, and T. Yamagata, 2017: Interbasin sources for two-year predictability of the multi-year La Niña event in 2010–2012. *Sci. Rep.*, **7**, 2276, https://doi.org/10.1038/s41598-017-01479-9.

Ma, J., S.-P. Xie, and H. Xu, 2017: Contributions of the North Pacific meridional mode to ensemble spread of ENSO prediction. *J. Climate*, **30**, 9167–9181, https://doi.org/10.1175/JCLI-D-17-0182.1.

Martín-Rey, M., B. Rodríguez-Fonseca, and I. Polo, 2015: Atlantic opportunities for ENSO prediction. *Geophys. Res. Lett.*, **42**, 6802–6810, https://doi.org/10.1002/2015GL065062.

McGregor, S., A. Timmermann, N. Schneider, M. F. Stuecker, and M. H. England, 2012: The effect of the South Pacific convergence zone on the termination of El Niño events and the meridional asymmetry of ENSO. *J. Climate*, **25**, 5566–5586, https://doi.org/10.1175/JCLI-D-11-00332.1.

——, N. Ramesh, P. Spence, M. H. England, M. J. McPhaden, and A. Santoso, 2013: Meridional movement of wind anomalies during ENSO events and their role in event termination. *Geophys. Res. Lett.*, **40**, 749–754, https://doi.org/10.1002/grl.50136.

McPhaden, M. J., and X. Zhang, 2009: Asymmetry in zonal phase propagation of ENSO sea surface temperature anomalies. *Geophys. Res. Lett.*, **36**, L13703, https://doi.org/10.1029/2009GL038774.

——, A. Santoso, and W. Cai, 2020: *El Niño Southern Oscillation in a Changing Climate*, *Geophys. Monogr.*, Vol. 253, Amer. Geophys. Union, 528 pp.

Meinen, C. S., and M. J. McPhaden, 2000: Observations of warm water volume changes in the equatorial Pacific and their relationship to El Niño and La Niña. *J. Climate*, **13**, 3551–3559, https://doi.org/10.1175/1520-0442(2000)013<3551:OOWWVC>2.0.CO;2.

Neale, R. B., and Coauthors, 2012: Description of the NCAR Community Atmosphere Model (CAM 5.0). NCAR Tech. Note NCAR/TN-486+STR, 274 pp., www.cesm.ucar.edu/models/cesm1.0/cam/docs/description/cam5_desc.pdf.

Neelin, J. D., D. S. Battisti, A. C. Hirst, F.-F. Jin, Y. Wakata, T. Yamagata, and S. E. Zebiak, 1998: ENSO theory. *J. Geophys. Res.*, **103**, 14 261–14 290, https://doi.org/10.1029/97JC03424.

Ohba, M., and H. Ueda, 2007: An impact of SST anomalies in the Indian Ocean in acceleration of the El Niño to La Niña transition. *J. Meteor. Soc. Japan*, **85**, 335–348, https://doi.org/10.2151/jmsj.85.335.

——, and ——, 2009: Role of nonlinear atmospheric response to SST on the asymmetric transition process of ENSO. *J. Climate*, **22**, 177–192, https://doi.org/10.1175/2008JCLI2334.1.

——, and M. Watanabe, 2012: Role of the Indo-Pacific interbasin coupling in predicting asymmetric ENSO transition and duration. *J. Climate*, **25**, 3321–3335, https://doi.org/10.1175/JCLI-D-11-00409.1.

Okumura, Y. M., 2019: ENSO diversity from an atmospheric perspective. *Curr. Climate Change Rep.*, **5**, 245–257, https://doi.org/10.1007/s40641-019-00138-7.

——, and C. Deser, 2010: Asymmetry in the duration of El Niño and La Niña. *J. Climate*, **23**, 5826–5843, https://doi.org/10.1175/2010JCLI3592.1.

——, M. Ohba, C. Deser, and H. Ueda, 2011: A proposed mechanism for the asymmetric duration of El Niño and La Niña. *J. Climate*, **24**, 3822–3829, https://doi.org/10.1175/2011JCLI3999.1.

——, P. N. DiNezio, and C. Deser, 2017: Evolving impacts of multiyear La Niña events on atmospheric circulation and U.S. drought. *Geophys. Res. Lett.*, **44**, 11 614–11 623, https://doi.org/10.1002/2017GL075034.

Planton, Y., J. Vialard, E. Guilyardi, M. Lengaigne, and T. Izumo, 2018: Western Pacific oceanic heat content: A better predictor of La Niña than of El Niño. *Geophys. Res. Lett.*, **45**, 9824–9833, https://doi.org/10.1029/2018GL079341.

Rayner, N. A., D. E. Parker, E. B. Horton, C. K. Folland, L. Alexandre, D. P. Rowell, E. C. Kent, and A. Kaplan, 2003: Global analyses of sea surface temperature, sea ice, and night marine air temperature since the late nineteenth century. *J. Geophys. Res.*, **108**, 4407, https://doi.org/10.1029/2002JD002670.

Rippey, B. R., 2015: The U.S. drought of 2012. *Wea. Climate Extremes*, **10**, 57–64, https://doi.org/10.1016/j.wace.2015.10.004.

Scaife, A. A., and Coauthors, 2014: Skillful long-range prediction of European and North American winters. *Geophys. Res. Lett.*, **41**, 2514–2519, https://doi.org/10.1002/2014GL059637.

Schott, F. A., S.-P. Xie, and J. P. McCreary, 2009: Indian Ocean circulation and climate variability. *Rev. Geophys.*, **47**, RG1002, https://doi.org/10.1029/2007RG000245.

Seager, R., and M. Hoerling, 2014: Atmosphere and ocean origins of North American droughts. *J. Climate*, **27**, 4581–4606, https://doi.org/10.1175/JCLI-D-13-00329.1.

Shukla, J., and Coauthors, 2000: Dynamical seasonal prediction. *Bull. Amer. Meteor. Soc.*, **81**, 2593–2606, https://doi.org/10.1175/1520-0477(2000)081<2593:DSP>2.3.CO;2.

Smith, R. D., and Coauthors, 2010: The Parallel Ocean Program (POP) reference manual. Los Alamos National Laboratory Tech. Rep. LAUR-10-01853, 140 pp.

Stuecker, M. F., A. Timmermann, F.-F. Jin, S. McGregor, and H.-L. Ren, 2013: A combination mode of the annual cycle and the El Niño/Southern Oscillation. *Nat. Geosci.*, **6**, 540–544, https://doi.org/10.1038/ngeo1826.

——, F.-F. Jin, A. Timmermann, and S. McGregor, 2015: Combination mode dynamics of the anomalous northwest Pacific anticyclone. *J. Climate*, **28**, 1093–1111, https://doi.org/10.1175/JCLI-D-14-00225.1.

Suarez, M. J., and P. S. Schopf, 1988: A delayed action oscillator for ENSO. *J. Atmos. Sci.*, **45**, 3283–3287, https://doi.org/10.1175/1520-0469(1988)045<3283:ADAOFE>2.0.CO;2.

Timmermann, A., and Coauthors, 2018: El Niño–Southern Oscillation complexity. *Nature*, **559**, 535–545, https://doi.org/10.1038/s41586-018-0252-6.

Trenberth, K. E., G. W. Branstator, D. Karoly, A. Kumar, N.-C. Lau, and C. Ropelewski, 1998: Progress during TOGA in understanding and modeling global teleconnections associated with tropical sea surface temperatures. *J. Geophys. Res.*, **103**, 14 291–14 324, https://doi.org/10.1029/97JC01444.

Vimont, D. J., J. M. Wallace, and D. S. Battisti, 2003: The seasonal footprinting mechanism in the Pacific: Implications for ENSO. *J. Climate*, **16**, 2668–2675, https://doi.org/10.1175/1520-0442(2003)016<2668:TSFMIT>2.0.CO;2.

Wallace, J. M., E. M. Rasmusson, T. P. Mitchell, V. E. Kousky, E. S. Sarachik, and H. von Storch, 1998: On the structure and evolution of ENSO related climate variability in the tropical Pacific: Lessons from TOGA. *J. Geophys. Res.*, **103**, 14 241–14 259, https://doi.org/10.1029/97JC02905.

Wang, C., and J. Picaut, 2004: Understanding ENSO physics—A review. *Earth's Climate: The Ocean-Atmosphere Interaction*, *Geophys. Monogr.*, Vol. 147, Amer. Geophys. Union, 21–48.

Wu, B., T. Li, and T. Zhou, 2010: Asymmetry of atmospheric circulation anomalies over the western North Pacific between El Niño and La Niña. *J. Climate*, **23**, 4807–4822, https://doi.org/10.1175/2010JCLI3222.1.

Wu, X., Y. M. Okumura, and P. N. DiNezio, 2019: What controls the duration of El Niño and La Niña events? *J. Climate*, **32**, 5941–5965, https://doi.org/10.1175/JCLI-D-18-0681.1.

Wyrtki, K., 1985: Water displacements in the Pacific and the genesis of El Niño cycles. *J. Geophys. Res.*, **90**, 7129–7132, https://doi.org/10.1029/JC090iC04p07129.

Xie, S.-P., and J. A. Carton, 2004: Tropical Atlantic variability: Patterns, mechanisms, and impacts. *Earth's Climate: The*

Ocean–Atmosphere Interaction, *Geophys. Monogr.*, Vol. 147, Amer. Geophys. Union, 121–142.

——, K. Hu, J. Hafner, H. Tokinaga, Y. Du, G. Huang, and T. Sampe, 2009: Indian Ocean capacitor effect on Indo-western Pacific climate during the summer following El Niño. *J. Climate*, **22**, 730–747, https://doi.org/10.1175/2008JCLI2544.1.

Yoo, S.-H., J. Fasullo, S. Yang, and C.-H. Ho, 2010: On the relationship between Indian Ocean sea surface temperature and the transition from El Niño to La Niña. *J. Geophys. Res.*, **115**, D15114, https://doi.org/10.1029/2009JD012978.

You, Y., and J. C. Furtado, 2017: The role of South Pacific atmospheric variability in the development of different types of ENSO. *Geophys. Res. Lett.*, **44**, 7438–7446, https://doi.org/10.1002/2017GL073475.

Zebiak, S., 1993: Air–sea interaction in the equatorial Atlantic region. *J. Climate*, **6**, 1567–1586, https://doi.org/10.1175/1520-0442(1993)006<1567:AIITEA>2.0.CO;2.